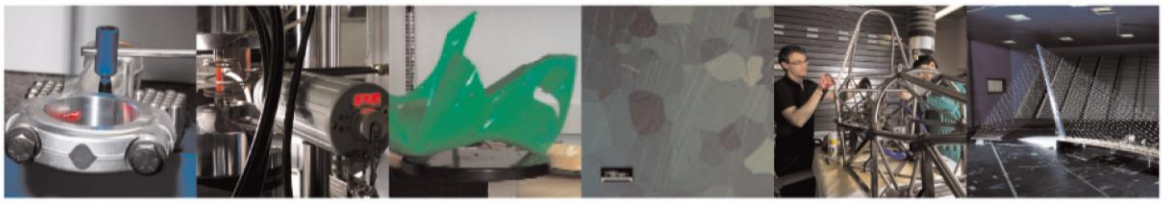

The influence of process variables on the gas forming and press hardening of steel tubes

Paul, Alexander; Strano, Matteo

DIPARTIMENTO DI MECCANICA ■ POLITECNICO DI MILANO
via G. La Masa, 1 ■ 20156 Milano ■ EMAIL (PEC): pecmecc@cert.polimi.it
http://www.mecc.polimi.it
Rev. 0

The influence of process variables on the gas forming and press hardening of steel tubes

Alexander Paul*, Matteo Strano**[1]

* Fraunhofer Institute for Machine Tools and Forming Technology IWU, Reichenhainer Straße 88, 09126 Chemnitz, Germany, alexander.paul@iwu.fraunhofer.de

** Politecnico di Milano, Dipartimento di Meccanica. Via La Masa 1, 20156 Milan, Italy, matteo.strano@polimi.it

Abstract

In this paper a study on the innovative process of hot tube metal gas forming and hot press hardening (Hot Metal Gas Press Hardening – HMG-PH) is presented. The aim is to provide new insights into the influence of process variables (gas pressure, tool temperature, tube pre-heating temperature, etc.) on the hardening phenomenon and on the quality of the produced tubular components (calibration radii, minimum wall thickness, etc.). Several experiments are described on two different kinds of steel, using a reference die geometry, specifically designed for investigating the typical critical issues of the process. The study demonstrates that the hardening phenomenon is strongly local not only because the hardness distribution is non-uniform over the final part, but especially because the hardening of different regions depends on different process parameters: in regions that need calibration, hardening is governed more by the pressure vs. time curve, i.e. by its rate and its maximum value and less by the tool temperature; in regions that rapidly go in contact to the die, hardening is governed more by the tool temperature and less by the pressure vs. time curve. Another relevant conclusion is that an optimal value of pressurization rate can be found that maximizes formability. Finally, the study proves that, on the formed tubes, obtaining small calibration radii and obtaining high values of hardness are conflicting objectives. The physical mechanisms behind these behaviours are discussed.

Keywords: Hot Metal Gas Forming; Press Hardening**;** Tube Hydroforming; 22MnB5; LH®800

[1] Corresponding author

1. Introduction

A strong trend towards using high-strength and super-high strength materials has established in car body designs. Press-hardened parts, with a maximum tensile strength of as much as 1900 MPa, play an important role because they are structural components, critical to crash performance. The main characteristic of the hot forming process of press-hardening is a combination of part shaping with a heat treatment taking place during the actual forming process. The benefits of press-hardening are evident both in the production phase (lower press forces, improved part shape accuracy and fewer forming steps due to higher true strain) and in the utilization phase (improved crash performance due to adapted component properties and lower component mass at the same level of stiffness). Using tubes and profiles offers further substantial potential for savings in terms of lightweight structural components.
Nevertheless, the process of hot press hardening for steel tubes, formed with internal pressure, is not yet widespread nor industrially established and more scientific and practical knowledge is strongly needed about this specific topic. As follows, a state of the art review is proposed about the process of forming a non-superplastic metal tube with internal pressure at elevated temperatures.
This topic has been scientifically investigated in the last 15 years, since when the Hot Metal Gas Forming (HMGF) research consortium was founded in the USA, with the aim of developing the process and proving its production readiness for widespread use in the automotive and aerospace industries (Dykstra, 2001). Since then, the scientific literature on hot internal forming of tubular steel, aluminium, titanium and magnesium alloys has focused on several lines of study: (1) the development of new tools and equipment and/or demonstration of case studies; (2) studies related to metallurgy and materials properties of incoming materials and formed products. Another important category of studies concerns process modelling, aimed at developing process design guidelines and studying the influence of process parameters. Process modelling is generally based on either (3) experimentally validated FEM simulations or (4) completely experimental studies.

1.1 Development of new tools and equipment, demonstration of case studies

As a clear indication that the process is still not mature and not industrially established, a large number of available papers focus, consistently over the years, on the proposal of new methods or systems or on the description of specific case studies. As an example, Zarazua et al. (2007) describe a prototype HMGF system for steel tubes; Yi et al. (2008) propose a new equipment for combined heating – comprised of an

induction coil plus a heating element – applied to the warm hydroforming of aluminium alloy tubes; Maeno et al. (2009) propose a machine for hot gas bulging process of aluminium alloys using resistance heating; Hwang et al. (2010) propose a machine for tube hydroforming of magnesium alloys at elevated temperatures; Sun and Smith (2010) propose a novel Closed-Volume Thermally Activated (CVTA) Tube Hydroforming method, obtained by conducting a high level of heat through the walls of a thick-walled, metallic, water-containing closed tube. Neugebauer et al. (2011) describe their tube press hardening method, developed for forming high strength steels. Recently, Maeno et al. (2014) propose a new gas forming process of ultra-high strength steel hollow parts using air filled into sealed tubes and resistance heating, developed in order to omit the subsequent heat treatment.

Case studies have been described by Keigler et al. (2005), where the prototyping of an aluminium tube made by temperature controlled hydroforming process is shown. In Schieck et al. (2010) magnesium wrought alloys and high-strength steels are used to demonstrate solutions and potentials for implementing tempered forming processes based on active media. Kenichiro Mori (2012) presents the hot stamping of a V-shaped steel tube using resistance heating.

1.2 Metallurgy and materials properties of incoming materials and formed products

Following another typical research line, several authors focus their attention on material-related issues. As an example, Yuan et al. (2006) present the results of hydro-bulging test carried out at elevated temperature on 5A02 aluminium tubes; Liu and Wu (2007) investigate by Electron Backscattered Diffraction (EBSD) and Electron Microscopy an AZ31 magnesium alloy tube has been deformed by HMGF. Elsenheimer and Groche (2009) describe a new testing technique, capable of realizing high process temperatures and constant strain rates. He et al. (2012) present the results of free bulging test carried out at high temperatures, to evaluate the formability of AA6061 extruded tubes.

1.3 Process modelling mainly based on numerical simulations

Simulation is a key topic within the development of the HMGF technology and its variants. Vadillo et al. (2007) simulate tube bulge tests and forming processes with dies of stainless and high strength steels. Grüner and Merklein (2010) study the accuracy of the Drucker-Prager Cap material model to describe tube hot forming with a granular medium. Seo et al. (2010) deal with the numerical modelling of hot press forming process of a boron steel tube. Hwang and Wang (2010) study the effects of loading paths with different feeding speed ratios and initial tube positions on the contact area at the counter punch

surface at the bulge stage, for y-shape tube hydroforming of magnesium alloys at elevated temperatures. D'Amours and Béland (2011) use LS-Dyna for modelling the warm forming of 7075 aluminium alloy tubes.

1.4 Process modelling mainly based on experimental campaigns

Not many studies are available, which thoroughly investigate the role of process parameters on an experimental basis. Nevertheless, this kind of knowledge is essential for the ultimate goal of developing reliable process design guidelines and enabling the development of the tube hot internal forming process. As one of the few examples, Liewald and Pop (2008) determine the maximum circumferential strain at different forming temperatures and strain rates of AZ31 tubes bulged in a die with square cross-section. Liu et al. (2010) also work on magnesium alloy tubes, studying the effects of temperature and axial feeding on the success of tube forming operations. Maeno et al. (2011) investigate the hot gas bulging process of an aluminium alloy tube, in order to optimize the axial feeding loading curve. Drossel et al. (2014) performed analytical and numerical calculations to study the influence of the active medium on the thermodynamics of the forming process of high strength steel tubes.

From the state of the art review an important lack of experimental data and studies clearly emerges. Comprehensive studies on the process phenomenology of hot tube metal gas forming and hot press hardening are still needed, in order to better understand the role of the most important process variables (gas pressure, tool temperature, tube pre-heating temperature, etc.) on the quality and the performance of the produced tubular components (surface hardness, calibration radii, minimum wall thickness, etc.). This paper is a contribution in filling this gap of knowledge.

2 Description of process and tool technology

To successfully integrate the heat treatment into the metal forming process based on active media it is necessary to pre-heat the incoming tube to a temperature higher than 840 °C. The thermal process guidance is closely driven by the process window for press-hardening of sheet metal components. The component parts built to date have been formed or calibrated with a maximum forming pressure of 70 MPa. A cycle time of 35 s was achieved in the experimental stage. Figure 1 shows the detailed process of the Hot Metal Gas Press Hardening (HMG-PH). This kind of forming process is a subgroup of Hot Metal Gas Forming (HMGF).

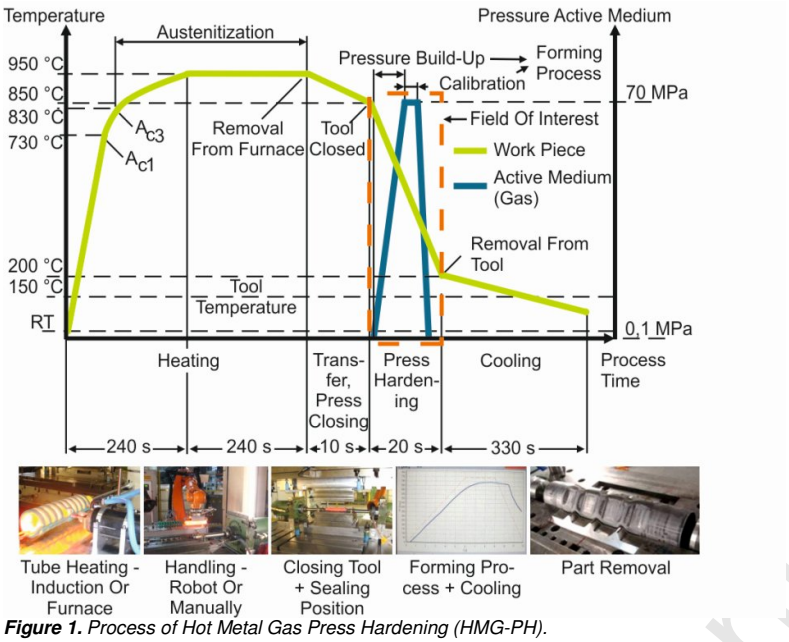

Figure 1. *Process of Hot Metal Gas Press Hardening (HMG-PH).*

Figure 2. *Hydroforming press Schuler SHP 50000 (left) and Maximator gas compressor (right).*

The experiments were performed with the hydraulic press Schuler SHP 50000 (Figure 2), which has a total press force of 50,000 kN and can transmit a force of up to 835 kN on the sealing punches. The maximum stroke of the axial cylinders is 300 mm. For our demonstrator is a closing force of 2.000 kN sufficient. The active medium nitrogen is compressed by the compressor unit Maximator ® RM/800/1/VP/240/800/So (Figure 2) up to 75 MPa and supplied to the tool without further tempering. The high pressure compressor has an accumulator with a volume of 20 l at a maximum adjustable

operating pressure of 75 MPa. The required gas inlet pressure has a range from 3 MPa to 30 MPa. The filling of the compressor with nitrogen was realized by a gas cylinder battery with an operating pressure of 30 MPa. The heating of the semi-finished products were done by using a chamber oven because the temperature in the oven is here well regulated.

With the experimental tool it was possible to carry out tests both with heated and cooled tools. In addition, the experimental tool was engineered in shell design to implement a close-contoured cooling system. Furthermore, the tool was heated with standard cartridge type heaters. These heating and cooling systems not only make it possible to study the impact that tool temperature has on the press-hardening process. They also make it possible to study tailored tempering for adjusting graded properties in the component part. Furthermore, the test tool was also equipped with devices for process monitoring and data recording. That means that the component part temperature can be measured with the metal forming process by installing a non-contact temperature measuring device via infrared sensor and a new type of measuring method via spring-loaded contact thermocouples. This makes it possible to record cooling-off curves over the entire process and gathers precise knowledge on the thermal behaviour of the component part and tool in the process. This is crucial for improving the modelling of the internal forming and press-hardening process including the reduction of the cycle time.

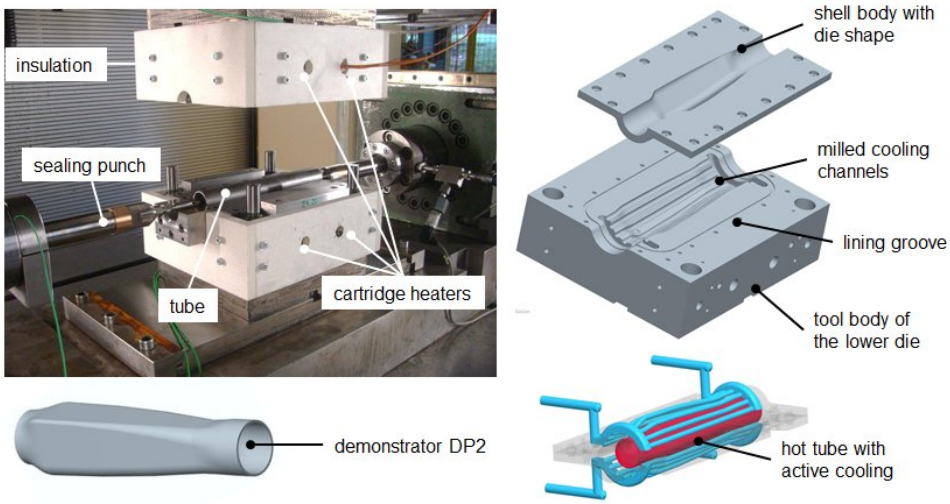

Figure 3. *Experimental tool in shell design with a cooling system close to the die surface and a heating system.*

The modular design should be assessed as non-critical as far as mechanical tool load from forming pressure is concerned. Forming at high temperatures causes a significant drop in the apparent yielding point of the materials to be formed, which brings about much lower forming pressures. Figure 3 shows a

hydroforming press-hardening tool in shell design, where the cooling duct cross-sections are inserted into the tool body and the tool shell on the half side.

2.1 Reference die shape design

The hot metal gas press hardening experimental tests have been planned with a reference part, shown in Fig. 4. Preliminary tests have been performed applying only the amount of axial feeding strictly required to seal the tube, because this process is very sensitive to the risk of wrinkles. The mechanics of the deformation process can therefore be described as a plain strain expansion, with the tube stretching in the hoop (circumferential) direction of an amount ε_h and a corresponding thinning approximately equal to $\varepsilon_t=-\varepsilon_h$, because of volume constancy. For this reason the cross-section with the largest risk of fracture during the process is D-D (Fig. 4), where the largest tube expansion takes place.

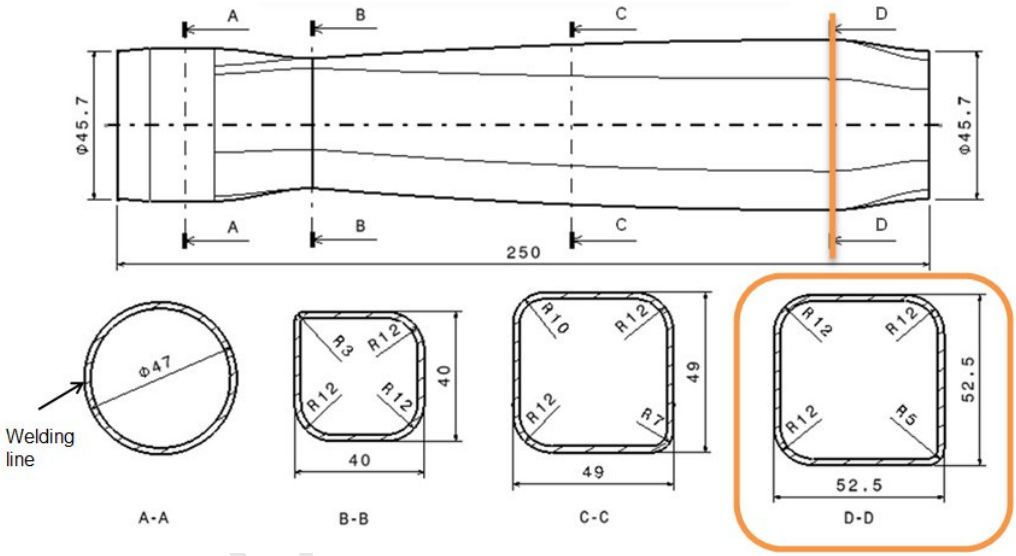

Figure 4. *Reference part for the experiments.*

The tested tubes have an initial outer diameter of 45 mm and a maximum calculated expansion of about 66 %, which would be impossible to reach with any steel at room temperature. The figure shows that one of the four corners of cross-section D-D has been designed with a smaller radius (5 mm instead of 12 mm). For this reason, the calibration process is not exactly symmetric and the occurrence of either fracture or insufficient calibration during the tests is always localised at the smaller R5 die radius. Since the tubes are welded and they are not heat treated before forming (they are only rapidly pre-heated), the welding line (which is fragile) has always be positioned away from the R5 location.

3 Experimental conditions

Two tube materials have been tested: LH®800 (wall thickness t_0= 1,55 mm) and 22MnB5 (t_0=1,50 mm). The LH®800 is a steel with original ferritic structure that transforms into austenite at elevated temperature and then, after air cooling, fully turns back into martensite. The 22MnB5 is a high strength cold-rolled boron steel, typical for hot stamping and press hardening automotive applications.

3.1 Process variables under investigation

A campaign of experiments has been planned with some process parameters under investigation (the "factors"), described as follows. The tube is pre-heated in a radiation furnace at a uniform temperature of T_{pr} [°C]. The tool must be pre-heated at temperature T_t [°C], in order to avoid a thermal shock to the tube when inserted in the die after pre-heating in the furnace. The temperature T_t or, alternatively, the difference $\Delta T = T_{pr} - T_t$ [°C] is the second factor. T_t or ΔT are important because they determine the cooling rate of the tube, hence they should primarily influence the hardening phenomenon. The internal gas is pressurized with an approximately linear pressure vs. time curve, up to a maximum calibration pressure P_{max} [MPa]. It can be expected that occurrence of fracture can be delayed and possibly avoided for smaller P_{max} values. However, if P_{max} is too small, the shape calibration may result insufficient. The time t_p [s] required for the gas pressure to build up from the beginning of the process until P_{max} is very important, because the pressurization rate determines the strain rate of the tube expansion, which strongly influences the material behaviour at elevated temperature. The fourth factor under control is therefore either the pressurization time t_p or the pressurization rate, i.e. the ratio P_{max}/t_p [MPa/s].

It can be expected that occurrence of fracture can be delayed and possibly avoided for slower P_{max}/t_p values, i.e. for smaller strain rates. However, as time goes by the tube keeps cooling down, deteriorating the material formability. As a consequence, the role of P_{max}/t_p is not trivial. The factors are listed in Table 1, where the experimental range is given, too.

		experimental range	
factors		**min**	**max**
pre-heating temperature	**T_{pr}** [°C]	950	1150
tool temperature or	**T_t** [°C]	100	400
tool-tube temperature difference	**ΔT** [°C]	550	1050
calibration pressure	**Pmax** [MPa]	30	60
pressurization time	**t_p** [s]	1	4
or rate	**P_{max}/ t_p** [MPa/s]	7.5	60

Table 1. *Experimental factors and range.*

3.2 Final hardness and product quality

Several response variables of interest have been considered and collected at the end of every experimental test: namely the risk of failure (by fracture), the final wall thickness distribution, the final calibration (i.e. die-tube distance), the minimum radius obtained, the final hardness distribution on the workpiece, etc. In this paper, however, only a subset of the most important response variables will be discussed, for brevity.

The risk of failure by fracture will be discussed first, as a dependent variable of the four factors listed in Section 3.1. Failure may occur at the welding line, if it is not correctly positioned, or at the corner R5 in the proximity of the cross-section D-D (see Fig. 4 and Fig. 5). The final wall thickness distribution can be measured throughout the whole workpiece but, again, the most interesting cross-section is the D-D. The smallest final thickness values are recorded in zone 4, i.e. in the proximity of radius R5. Since the factors that lead to the thinning phenomenon, in a plane strain deformation as the present test case, are expected to play the same role in the fracture phenomenon, any further consideration about thinning are avoided in the remainder of the paper and the focus will rather be on the risk of fracture. The response variable P_s=1- P_f will be used, where P_s is the probability of a part being safe at the end of the forming process and P_f is the probability of a part being failed.

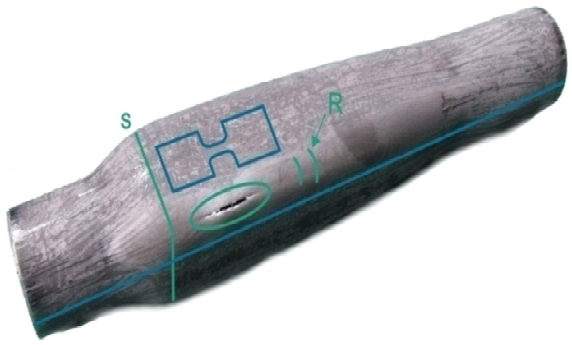

Figure 5. *Typical location of fracture.*

The calibrating ability of the process can be estimated by measuring the final values of the actual minimum radii obtained on the formed tubes. The two measurement locations of interest are in zone 4 at the cross-section D-D in Figure 4 (where the target radius is 5 mm and there is a large tube expansion) and at the cross-section B-B of figure 4, where one of the four die corners has a target minimum value of 3

mm but there is a small tube expansion. Two response variables will be considered in the results, [mm] and R_B [mm], the final minimum radii measured respectively at cross-sections B-B and D-D.

The final hardness of the part is a clear measure of the effectiveness of the tempering process due to air cooling. Since the final hardness depends on the local stress-strain-temperature history of each tube location, there is a non-uniform distribution of hardening throughout the part. The actual cooling rate will probably depend also on how fast the process is performed (i.e. on t_p) and on how cool is the tool surface with respect to the tube temperature (i.e. on T_t or ΔT). If the 5 zones that describe the cross-section D-D are considered (shown in the right part of Fig. 6), the area where the lowest cooling rate can be expected is the smaller corner, zone 4, where the tube never completely touches and exchanges heat with the die. The rest of the tube perimeter rapidly touches the die and exhibits approximately the same hardness values (see the profiles in Fig. 6). Vickers hardness measurements HV_2 (taken at the centre of the corner zone 2) and HV_4 (taken at the centre of the corner zone 4) can represent the effect of the air hardening process after forming. Vickers hardness measurements HV_1, HV_3 and HV_5 (taken at the centre of flat zones, in rapid contact with the dies) can represent the effect of the press hardening process after forming.

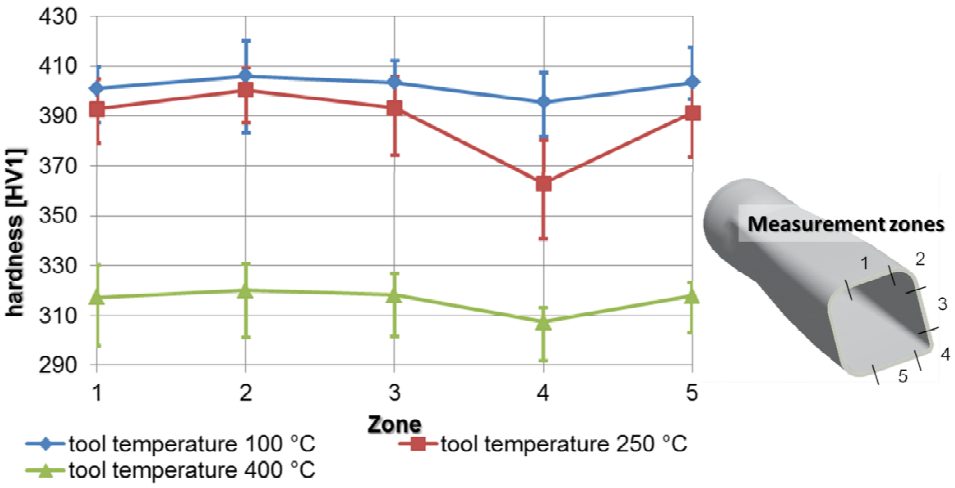

Figure 6. *Examples of final HV hardness distribution at cross-section D-D in five measurement locations, grouped by tool temperature; error bars are also shown around the data points.*

4 Results and discussion of experimental plans

Three separate experimental plans have been conducted: I) an experimental plan for determining the influence of factors on the probability of failure and success, using material LH®800; II) an experimental

plan on material LH®800, for determining the significance of the factors on hardening and calibration parameters; III) an experimental plan on material 22MnB5, for verifying again the significance of the factors on hardening and calibration parameters with a different material.

4.1 The influence of parameters on the risk of fracture

In order to analyse which factors are involved in failure by fracture in LH®800 tubes, a statistical tool was used (the Binary logistic regression model) that allows to use a regression on a binary type variable (takes the value 1, if the tube is safe; takes the value 0, if the tube is fractured). The results of this regression analysis allow to calculate the probability of the event depending on the factors. The parameters to be estimated are the coefficients (Coef) $\beta_0, \beta_1, \beta_2, \ldots, \beta_a$ of the formula:

$$Prob_{succes}[\%] = \frac{e^{\beta_0+\beta_1 x_1+\beta_2 x_2+\cdots}}{1+e^{\beta_0+\beta_1 x_1+\beta_2 x_2+\cdots}} \quad (1)$$

which gives the probability of a part being safe, as a function of the factor variables x_1, x_2, etc. Equation (1) is called "logit" link function. Among the numerous considered potential factors listed in Section 3.1, four of them were included in the final model described in the Table 2 and Figure 7. The model has been built over 52 experimental observations, with process parameters in the range previously given in Table 1.

Binary Logistic Regression							
Factors	**Coefficients**	**Std. Err. of Coef.**	**Z**	**P-value**	**Ratio**	**Lower**	**Upper**
Constant	6,249	2,547	2,450	0,014			
P_{max}	-0,329	0,012	-2,660	**0,008**	0,970	0,940	0,990
T_{pr}	1,001	0,811	1,230	0,218	2,720	0,550	13,340
P_{max}/t_p	0,196	0,010	1,880	**0,060**	1,020	1,000	1,040
deltaT	-0,002	0,002	-0,840	0,402	1,000	0,990	1,000

Log-Likelihood =	-23.368		
Test that all slopes are zero:	**G statistic**	**Degrees of Freedom (DoF)**	**P-value**
	25.351	4	0.000
Pearson Goodness-of-Fit Tests	**χ^2 statistic**	**DoF**	**P-value**
	57.3931	40	0.037

Measures of Association Between the Response Variable and Predicted Probabilities				
Pairs	Number	Percent	Summary Measures	
Concordant	605	89.5	Somers' D	0.79
Discordant	71	10.5	Goodman-Kruskal Gamma	0.79
Ties	0	0.0	Kendall's Tau-a	0.40

Table 2. *Binary logistic regression table for the probability of a LH®800 part being safe.*

Table 2 shows that the only factors that influence bursting are the target maximum pressure P_{max} (P-value 0.008, i.e. a probability of the factor being significant is 0.992) and the target pressurization ratio P_{max}/t_p (P-value 0.06). The difference in temperature between the furnace and the tool deltaT and the actual build-up time t_{pr} both help improving the goodness-of-fit of the model but they are not statistically significant (P-value > 0.1). The goodness-of-fit tests are positive. The diagnostic measures of the model

are very good, with a high Somers' D number (equal to 0.79) and a concordance in the prediction of 89.5 %. More details on the statistical issues of this type of model can be found in (McCullagh and Nelder, 1992).

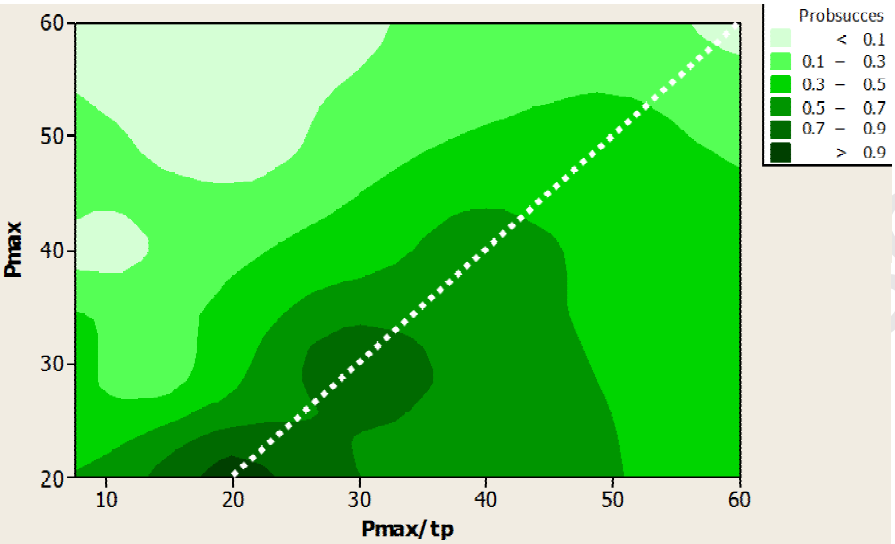

Figure 7. *Probability of success depending on maximum pressure (MPa) and pressurization speed (MPa/s) for LH®800 tubes.*

Figure 7 shows the formability map, according to the resulting equation (2), including the two aforementioned significant factors, where darker areas indicate safer zones.

$$Prob_{succes}[\%] = \frac{e^{6,249-0,329F_{max}+1,001T_{pr}+0,196\frac{F_{max}}{t_p}-0,002deltaT}}{1+e^{6,249-0,329F_{max}+1,001T_{pr}+0,196\frac{F_{max}}{t_p}-0,002deltaT}} \quad (2)$$

The probabilities of a part being safe tend to decrease if P_{max} increases, as expected.

Discussion of observed behaviours. Interestingly, there is a non-linear relationship with the pressurization rate since, for every P_{max} value, there is an optimal value of P_{max}/t_p that maximizes formability, approximately represented by the dotted line in Figure 7, drawn according to the regression model. This behaviour can be physically explained because slower pressurization rates allow for the tube to cool down and reduce its formability, whereas higher pressurization rates induce greater and more dangerous strain rates on the tube. The safer regions are very narrow, indicating that the process must be carefully designed to ensure robustness. The metallurgy of LH800 helps explain this behaviour: as received, it exhibits a single-phase ferrite grain microstructure. When heated above 950 °C, it transforms into austenite. When cooling down, martensite forms leaving a mixed ferritic-martensitic structure. The martensitic structure is harder but more fragile, with less formability. If the deformation is too slow (slow

pressurization), the material has time to form fragile martensite. On the other hand, some authors have demonstrated that ferritic-martensitic steels have a non-linear behaviour with respect to strain rate, i.e. there is an optimal strain rate that maximizes elongation at fracture in the 300-800 °C temperature range (Vanaja et al., 2012). A non-linear behaviour with respect to strain rates have been found not only for steels, but also for other alloys, e.g. the aluminium alloy 8085 (Bruschi et al., 2013).

4.2 The effect of process variables on hardness

A regression model (GLM, General Linear Model) has been built over the experimental results obtained on the LH®800 tubes, in order to verify which factors mostly influence the response the hardness at the different zones shown in Fig. 6. The experiments have been conducted by changing four experimental factors at two or three levels: tool temperature Tt (150, 250 and 400 °C), calibration pressure P_{max} (30 and 40 MPa), tube pre-heating temperature T_{pr} (950 and 1150 °C), pressurization time t_p (1, 2.5 and 4 s). If all factors are tested and combined with all levels of the remaining three factors, 36 conditions would be necessary. However, most of these combinations cannot be tested because they yield failed tubes (because of largely insufficient calibration or fracture). Only 11 useful conditions could be tested; some tests have been replicated for a total of 18 measured tubes. Figure 6 already shows how the tool temperature influences the hardness reached in the 5 different regions of the workpiece. It is now useful to deepen the analysis focusing on regions 3 and 4, which well represent respectively the hardening in contact with the die and the air hardening (at the corner).

Hardness at the corner. The results have been partially already shown in Fig. 6. If the hardness at the corner regions is considered, it is mostly influenced by the tool temperature T_t and the calibration pressure P_{max}, and not influenced at all by t_p. A predictive model for HV_4 has been built including also the tube pre-heating temperature T_{pr}, which improves the goodness-of-fit of the regression model. The results are summarised in Table 3, where the coefficients (second column) indicate the sign of the relation between each factor and the final hardness, while the P-values denote if the relation is statistically significant. Another experimental plan has been conducted using the 22MnB5 tubes. The results are very similar to the LH®800 case and confirm that HV_4 is influenced mainly by P_{max} and tool temperature.

If looking at the indications of the model, higher pressure values lead to more compressed and therefore harder tube corners. The tool temperature negatively influences HV_4. It can be easily assumed that when

the tube comes in contact with a colder die, the tempering process is faster and deeper and a superior hardness is achieved.

General Regression Analysis: HV Zone 4 versus T_t, P_{max}, T_{pr}				
Term	**Coefficients**	**Std. Err. of Coef.**	**T statistic**	**P-value**
Constant	303,276	45,857	6,614	0,000
T_t	-0,265	0,019	-14,284	**0,000**
P_{max}	2,316	0,053	4,363	**0,001**
T_{pr}	0,045	0,037	1,227	0,240
S	**R^2**	**R^2 adjusted**		
8,753	95,88 %	95,00 %		

$$HV_4 = 303{,}276 - 0{,}265\,T_t + 2{,}316 P_{max} + 0{,}045\,T_{pr}$$

Table 3. *Linear regression table for the hardness in the corner zone 4 of LH®800 parts.*

Hardness at the flat regions. As for HV_4, a similar and even stronger effect of tool temperature T_t can be observed on the response variable HV_3, the hardness at the flat zone, which comes in contact to the die earlier than the corners. Colder dies produce harder tubes. On the contrary, the role of calibration P_{max} and tube pre-heating temperature T_{pr} is here totally negligible. The tempering effect starts and develops earlier, when the pressure values are still far from calibration, and when P_{max} is reached the hardening process has already taken place. Similarly, the cooling effect of the dies makes the effect of the pre-heating temperature negligible in the considered experimental range.

The role of the pressure build-up time t_p is interesting: it is not statistically very significant, but it has a weak effect: if included in the regression model it helps improving the goodness of fit, as shown by the regression model described in Table 4, developed on the LH®800 experiments.

Similar results have been found on the 22MnB5 tests: strong influence of tool temperature T_t, weak influence of pressurization time t_p, no influence of P_{max} (T_{pr} has not been investigated in 22MnB5 tests). Greater hardness values on the flat regions can be achieved with small build-up times and low tool temperatures.

General Regression Analysis: HV Zone 3 versus T_t; T_t^2; t_p				
Term	**Coefficients**	**Std. Err. of Coef.**	**T statistic**	**P-value**
Constant	372,070	993,984	374,322	0,000
T_t	0,426	0,100	42,449	**0,001**
T_t^2	-0,001	0,000	-71,864	**0,000**
t_p	3,437	212,752	16,154	**0,129**

S	R^2	R^2 adjusted
8.56312	95.96%	95.09%

$$HV_3 = 372.07 + 0.4256\ T_t - 0.0015\ T_t^2 + 3.4370\ t_p$$

Table 4. *Linear regression table for HV_3 of LH®800 parts.*

Discussion of observed behaviours. It is very interesting that the hardening phenomenon not only is strongly local because of a non-uniform hardness distribution, but especially because the hardening of different regions depend on different factors. In corner regions, where the tube freely expands for a long process time and comes in contact to the die only at the calibration phase, the hardening phenomenon is governed by the pressure vs. time curve, i.e. by its rate and its maximum value. In flat regions, where contact to the die surfaces is rapid, the hardening phenomenon is governed by the tool temperature vs. time curve, i.e. by its initial and by the time required to complete the forming process. Noticeably, these considerations apply to both investigated steel materials.

4.3 The effect of process parameters on the calibration radii

The radius R_D in cross-section D-D (see Figure 4) is resulted the most difficult corner to be calibrated. A GLM has been built on the LH®800 first plan, indicating that the most important parameter is the maximum pressure P_{max}, followed by the pre-heating temperature T_{pr}. If pressure and tube temperature increase, the achieved radius gets smaller. This result is not surprising, but it is more important to observe that the tool temperature T_t has a weak but not totally negligible effect, as shown by the P-values in Table 5. As the tool temperature increases, it gets more difficult to obtain small radii.

General Linear Model: R_{min} versus T_t; P_{max}; t_p; T_{pr}						
Factor	**Unit**	**Type**	**Levels**	**Values**		
T_t	°C	fixed	3	100; 250; 400		
P_{max}	MPa	fixed	2	30; 40		
t_p	s	fixed	3	1,0; 2,5; 4,0		
T_{pr}	°C	fixed	2	950; 1150		
Analysis of Variance for R_{min}, using Adjusted SS for Tests						
Source	**Degrees of Freedom (DoF)**	**Sequential Sum of Squares (SS)**	**Adjusted SS**	**Adj Mean Square Error**	**F statistic**	**P-value**
T_t	2	11,021	1,706	0,853	3,040	0,089
P_{max}	1	5,307	5,810	5,810	20,690	**0,001**
t_p	2	1,314	1,141	0,570	2,030	0,178
T_{pr}	1	2,724	2,724	2,724	9,700	**0,010**
Error	11	3,090	3,090	0,281		
Total	17	23,456				
S	**R^2**	**R^2 adjusted**				
0,530	86,83 %	79,64 %				

Table 5. *Linear regression table for R_D of LH®800 parts.*

This non trivial behaviour, i.e. the small but not totally negligible influence of tool temperature T_t has been confirmed also by the test run on the 22MnB5 tubes (Table 6).

General Linear Model: R_{max}; R_{min} versus P_{max}; T_t			
Factor	Type	Levels	Values
P_{max}	fixed	4	30; 40; 50; 60
T_t	fixed	4	100; 250; 325; 400
t_p	covariate	3	1; 2.5; 4

Analysis of Variance for R_{min}, using Adjusted SS for Tests						
Source	**DoF**	**Sequential Sum of Squares (SS)**	**Adj SS**	**Adj MSE**	**F statistic**	**P-value**
P_{max}	3	14,456	14,730	4,910	54,340	**0,000**
T_t	3	1,696	1,457	0,486	5,370	**0,016**
t_p	1	0,057	0,057	0,057	0,630	0,444
Error	11	0,994	0,994	0,090		
Total	18	17,203				
S	**R^2**	**R^2 adjusted**				
0,301	94,22 %	90,55 %				

Table 6. *Linear regression table for R_D of 22MnB5 parts.*

Discussion of observed behaviours. The results on the minimum radius clearly show that, as in conventional hydroforming, calibration strongly and obviously depends on the maximum pressure. They also show that when the tubes are initially warmer, calibration is easier as the material is softer. For similar reason, calibration is easier when the dies are hotter, i.e. when they keep warm and soft the workpiece for a longer time. Noticeably, these considerations apply to both investigated steel materials. The reason is probably due to a more rapid cooling (i.e. hardening) of the tubes when the dies are colder, and this makes more difficult to obtain a good calibration.

5 The interaction between pressure and tool temperature

The experimental plans in Section 4 showed the main effects of the factors, i.e. what process parameters are significant (or not significant) over the probability of failure, the hardness of the parts, the calibration radii. In general, pressure and tool temperature are the two factors that most frequently and most significantly have an influence on the process responses. For this reason, a fourth, deeper and more focused experimental plan has been conducted, aimed at building a model centred on these two parameters and show how they interact.

In Section 4, we have shown that for both steel materials under investigation, the role played by the factors is very similar. For this reason, this fourth plan has been conducted on only one type of incoming material (LH®800 tubes with 2,05 mm wall thickness) and has been designed in order to include in the

models any potentially influent quadratic and interaction term. For this purpose, a Central Composite Design (CCD) has been selected, which is quite robust with respect to the possibility of missing data, due to potential fracture of some samples (Tanco et al., 2013). The CCD design (described in Figure 8) has been analysed by means of a Response Surface Analysis.

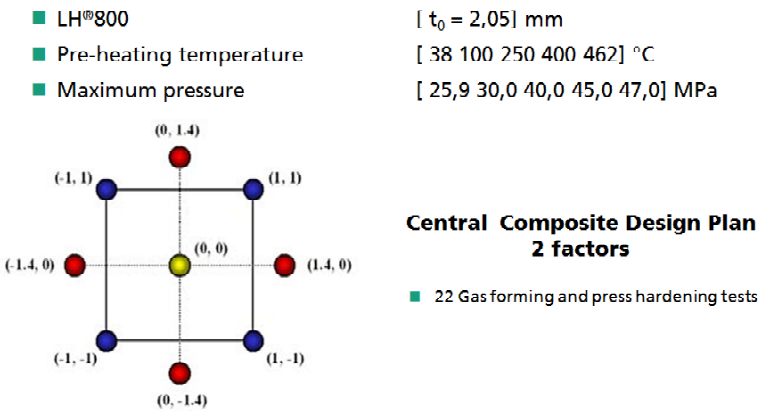

Figure 8. *CCD for final tests.*

Hardness at the flat surfaces. It has been measured by the parameter HV_{135}, which is the average of surface hardness at zones 1, 3 and 5 in cross-section D-D. The corresponding response surface model is plotted in Figure 9. The mentioned figure (and the underlying response regression analysis, here omitted for brevity) indicates a strong non-linear (quadratic) dependence on the tool temperature T_t and a mild linear and square dependence on the pressure P_{max} (which went undetected in the screening plans shown in Section 4.2).

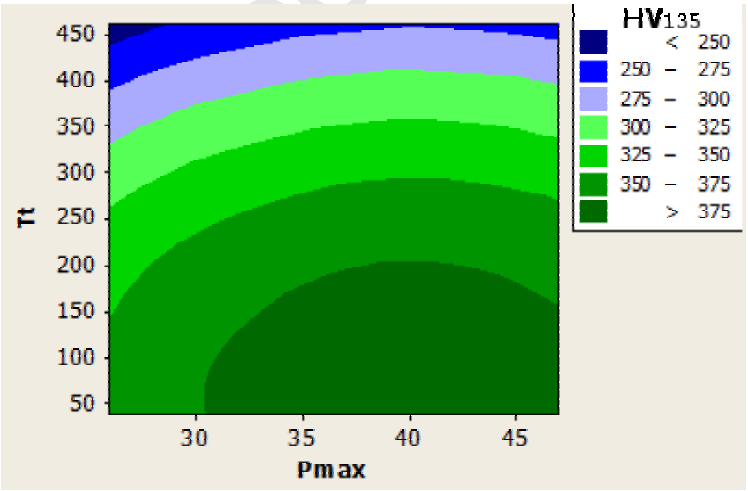

Figure 9. *Response surface of the CCD plan for hardness HV_{135} on the flat regions.*

Hardness at the corners. It has been measured by the parameter HV_{24}, which is the average of surface hardness at zones 2 and 4 in cross-section D-D. The corresponding response surface model is plotted in Figure 10. The mentioned figure (and the underlying response regression analysis) indicates that all investigated factors and interactions are significant. These results are in agreement and further confirm the screening tests presented in Section 4.3.

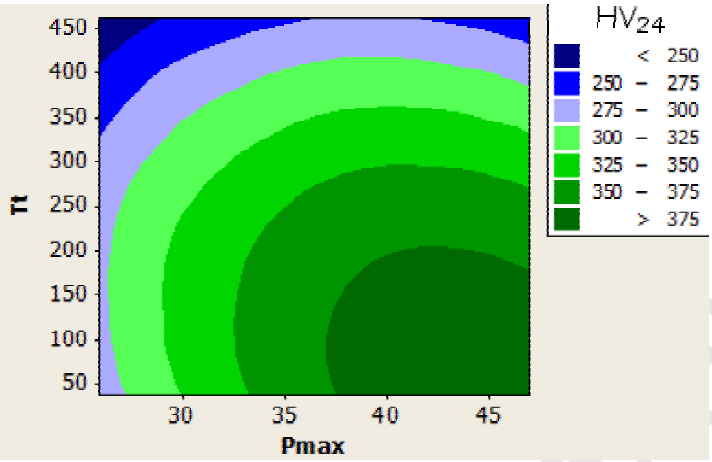

Figure 10. *Response surface of the CCD plan for hardness HV_{24} on the corners.*

Minimum calibration radius. It has been measured by the parameter R_D, as in Section 2. The corresponding response surface model is plotted in Figure 11. The mentioned figure (and the underlying response regression analysis) indicates that the maximum pressure and the square of the tool temperature are significant. These results are in agreement and further confirm the screening tests presented in Section 4.3.

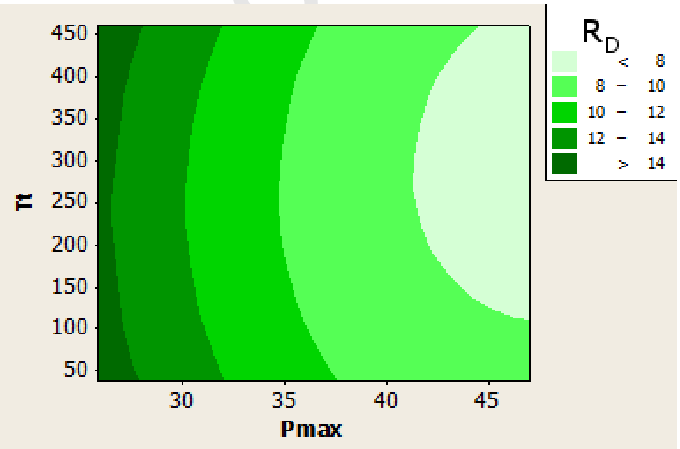

Figure 11. *Response surface of the CCD plan for R_D on the flat regions.*

***Discussion of observed behaviours*.** The results on hardness clearly confirm the results and discussion of Section 3, but they interestingly show how pressure and tool temperature interact in a different way in different regions of the dies. In the corners, where contact to the dies occurs at the end of the process, smaller hardness values can be measured, because the thermal gradient between the tube and the contacted portion of die is progressively reduced. The hardening phenomenon is governed more by pressure and less by the tool temperature. On the contrary, in the flat sides, that rapidly go in contact to the die, larger hardness values can be measured. The hardening phenomenon is governed more by the initial tool temperature and much less by the maximum pressure reached.

6 Conclusions

Four comprehensive experimental plans have been conducted and analysed in order to investigate the role of the main process parameters of the gas forming and press hardening process (Hot metal gas press hardening - HMG-PH) for steel tubes. Empirical models have been developed for predicting the occurrence of fracture, the final tube hardness and the calibration radii. The main conclusions can be summarised as follows.

As the process was performed with no axial feeding of the tubes, the main risk of failure is their premature fracture, before calibration has been accomplished. The risk of fracture is influenced not only by the maximum target pressure of the process (as it is obvious), but also by the pressurization rate. As a very interesting result, an optimal value of pressurization rate can be found that maximizes formability. This can be physically explained because very low pressurization rates allow for the tube to cool down and reduce its formability; on the other hand, very high pressurization rates induce greater and more dangerous strain rates on the tube.

The final hardness induced on the tube is not uniformly distributed: in regions that need calibration (e.g. the corners of a square or rectangular tube), where contact to the dies occurs at the end of the process, smaller hardness values can be measured, because the thermal gradient between the tube and the contacted portion of die is relatively low. The hardening phenomenon is governed more by the pressure vs. time curve, i.e. by its rate and its maximum value and less by the tool temperature.

In regions that rapidly go in contact to the die (e.g. the flat sides of a square or rectangular tube), larger hardness values can be measured. The hardening phenomenon is governed more by the tool temperature and less by the pressure vs. time curve.

The minimum achievable radii, as in conventional hydroforming, obviously depend on the maximum pressure. As for the other process parameters, unfortunately, when they have a positive effect on the final tube hardness, at the same time they have a negative effect on calibration, i.e. on the chances of obtaining small radii. A compromise solution must therefore be found between geometrical complexity and final part strength.

7 Acknowledgments

The IGF project 16961 BR of the European Research Association for Sheet Metal Working was funded by the German Federal Ministry for Economics and Technology through the AiF in the framework of the programme for funding industrial community research (IGF) based on a decision of the German Federal Parliament. Fraunhofer IWU would like to extend its thanks to its project partners for their cooperation and support in this project.

The authors wish to acknowledge the work of Mr. Nicolò Vecchi, who gave a great contribution in the design of the experimental conditions and in the actual conduction of the experimental tests.

References

Bruschi, S., Ghiotti, A., Michieletto, F., 2013. Hot Tensile Behavior of Superplastic and Commercial AA5083 Sheets at High Temperature and Strain Rate. Key Eng. Mater. 554-557, 63–70.

D'Amours, G., Béland, J.F., 2011. Warm forming simulation of 7075 aluminium alloy tubes using LS-DYNA. In: 8th European LS-DYNA Users Conference. Strasbourg, pp. 1–12.

Drossel, W.-G., Pierschel, N., Paul, A., Katzfuß, K., Demuth, R., 2014. Determination of the active medium temperature in media based press hardening processes. J. Manuf. Sci. Eng. 136, 021013.

Dykstra, B., 2001. Hot Metal Gas Forming. Met. Form. 50–52.

Elsenheimer, D., Groche, P., 2009. Determination of material properties for hot hydroforming. Prod. Eng. 3, 165–174.

Grüner, M., M. Merklein, 2010. Numerical simulation of hydro forming at elevated temperatures with granular material used as medium compared to the real part geometry. Int. J. Material Form. 3, 279-282.

He, Z., Fan, X., Shao, F., Zheng, K., Wang, Z., Yuan, S., 2012. Formability and microstructure of AA6061 Al alloy tube for hot metal gas forming at elevated temperature. Trans. Nonferrous Met. Soc. China 22, s364–s369.

Hwang, Y.-M., Su, Y.-H., Chen, B.-J., 2010. Tube hydroforming of magnesium alloys at elevated temperatures. J. Eng. Mater. Technol. 132, 031012.

Hwang, Y.M., Wang, K.H., 2010. Study on y-shape tube hydroforming of magnesium alloys at elevated temperatures. Int. J. Mater. Form. 3, 175–178.

Keigler, M., Bauer, H., Harrison, D., De Silva, A.K.M., 2005. Enhancing the formability of aluminium components via temperature controlled hydroforming. J. Mater. Process. Technol. 167, 363–370.

Liewald, M., Pop, R., 2008. Magnesium tube hydroforming. Materwiss. Werksttech. 39, 343–348.

Liu, Y., Wu, X., 2007. A microstructure study on an AZ31 magnesium alloy tube after hot metal gas forming process. J. Mater. Eng. Perform. 16, 354–359.

Maeno, T., Mori, K., Adachi, K., 2014. Gas forming of ultra-high strength steel hollow part using air filled into sealed tube and resistance heating. J. Mater. Process. Technol. 214, 97–105.

Maeno, T., Mori, K., Fujimoto, K., 2009. Development of the hot gas bulging process for aluminium alloy tube using resistance heating. Key Eng. Mater. 410-411, 315–323.

Maeno, T., Mori, K., Unou, C., 2011. Optimisation of condition in hot gas bulging of aluminium alloy tube using resistance heating set into dies. Key Eng. Mater. 473, 69–74.

McCullagh, P., Nelder, J.A., 1992. Generalized Linear Models, Chapman & Hall.

Mori, K., 2012. Smart hot stamping of ultra-high strength steel parts. Trans. Nonferrous Met. Soc. China 22, s496–s503.

Neugebauer, R., Schieck, F., Werner, M., 2011. Tube press hardening for light weight design. In: ASME 2011 International Manufacturing Science and Engineering Conference, Corvallis, USA., pp. 495-502.

Schieck, F., Paul, A., Prohl, M., Cz, P., Pröhl, M., 2010. Forming technologies in automotive industry by applying lightweight materials. In: COMAT 2010. Pilsen.

Seo, O.S., Yoon, S.J., Suh, C.H., Kim, H.Y., Barlat, F., Moon, Y.H., Lee, M.G., 2010. Numerical modeling of hot press forming process of boron steel tube. In: American Institute of Physics Conference Series, pp. 1216–1222.

Sun, X., Smith, L.M., 2010. External heating closed-volume thermally activated tube forming: A fundamentally new approach for hydroforming thick-walled tubes. J. Manuf. Process. 12, 63–66.

Tanco, M., del Castillo, E., Viles, E., 2013. Robustness of three-level response surface designs against missing data. IIE Trans. 45, 544–553.

Vadillo, L., Santos, M.T., Gutierrez, M.A., Pérez, I., González, B., Uthaisangsuk, V., Pérez, I., González, B., 2007. Simulation and experimental results of the hot metal gas forming technology for high strength steel and stainless steel tubes forming. In: Proceedings of the 9th NUMIFORM Conference. AIP, Porto, pp. 1199–1204.

Yi, H.K., Pavlina, E.J., Van Tyne, C.J., Moon, Y.H., 2008. Application of a combined heating system for the warm hydroforming of lightweight alloy tubes. J. Mater. Process. Technol. 203, 532–536.

Zarazua, J.I., Vadillo, L., Mangas, A., Santos, M., Gutierrez, M., Gonzalez, B., 2007. Alternative Hydroforming Process for High Strength and Stainless Steel Tubes in the Automotive Industry. In: International Deep-Drawing Research Group IDDRG International Conference. Gyor, Hungary.

List of figure captions

Figure 1. *Process of Hot metal gas press hardening (HMG-PH).*

Figure 2. *Hydroforming press Schuler SHP 50000 (left) and Maximator gas compressor (right).*

Figure 3. *Experimental tool in shell design with a cooling system close to the die surface and a heating system.*

Figure 4. *Reference part for the experiments.*

Figure 5. *Typical location of fracture.*

Figure 6. *Examples of final HV hardness distribution at cross-section D-D.*

Figure 7. *Probability of success depending on maximum pressure (MPa) and pressurization speed (MPa/s) for LH®800 tubes.*

Figure 8. *CCD for final tests.*

Figure 9. *Response surface of the CCD plan for hardness HV_{135} on the flat regions.*

Figure 10. *Response surface of the CCD plan for hardness HV_{24} on the corners.*

Figure 11. *Response surface of the CCD plan for R_D on the flat regions.*